OPTIMIZATION OF AIR SOURCE HEAT PUMP SYSTEM BASED ON TRNSYS AND ARTIFICIAL NEURAL NETWORK

Qi Zhao[1, *], Wende Wu[2], Shijie Gu[1], Xiaoyue Liu[3], Bo Tian[1], Bowen Chu[1], Shuang Ma[1], Hongwen Jin[1]

[*1]School of Energy and Power, Changchun Institute of Technology, Changchun 130012, China

[2] Urban Construction College, Changchun University of Architecture and Civil Engineering, Changchun 130604, China

[3]School of Energy and Environmental Engineering, Jilin University of Architecture and Technology, Changchun 130114, China

[*] Corresponding author; E-mail: 0211037@ccit.edu.cn

This study proposes a hybrid neural network architecture that integrates error backpropagation (EBP) optimization with TRNSYS co-simulation, specifically targeting the performance enhancement of air-source heat pump (ASHP) systems in public buildings. The calculated optimal dynamic return water temperature setting was input into an established low-temperature air-source heat pump model for feasibility verification. Results showed: fan energy consumption rose by 13.0% vs. the traditional control method, while unit energy consumption dropped by 8.60% and per-unit-area system energy consumption decreased by 6.99%. The optimized method was applied to a typical air-source heat pump heating system in Changchun during the heating period on high-conditioning days. In low-conditioning mode, daily energy consumption fell from 287 kW·h (traditional) to 262 kW·h (optimized) – an 8.7% reduction. In high-conditioning mode, it decreased from 737.3 kW·h to 710.5 kW·h, a 3.6% drop. When used in three typical such systems across three cities in severely cold regions, the optimized method cut per-unit-area unit energy consumption by 5.15%-9.31% and per-unit-area system energy consumption by 6.15%-7.37% compared to the traditional method. By dynamically controlling the optimal return water temperature of the simulation system, energy consumption has been reduced, which has contributed value to achieving China's dual carbon goals.

Key words*: air source heat pump; TRNSYS; Artificial Neural Network; Operation optimization; Saving energy*

1. Introduction

Reducing carbon dioxide emissions has emerged as a critical strategic priority for nations

worldwide. China has committed to achieving carbon peaking by 2030 and carbon neutrality by 2060[1], with particular urgency given that the building sector ranks among the nation's three most energy-intensive industries[2]. Operational building activities in China generated substantial carbon emissions in 2020, comprising: 1) Direct emissions: 550 million tons of CO_2 (25% of total sector emissions)

2) Indirect emissions from electricity consumption: 1.15 billion tons of CO_2 (53%)

3) Heat-related emissions: 470 million tons of CO_2 (22%)[3]

In recent years, the advantages of using low-heat sources and a pollution-free environment of air source heat pump (ASHP) have attracted more and more attention[4]; however, their operational efficiency in cold climates remains constrained by frost accumulation[5]. So many scholars have realized the efficient operation of the ASHP system by integrating the system and using other renewable energy sources, and achieved relatively good results, and found that hybridization with renewable energy demonstrates significant potential. Yubo Wang et al[6] integrated solar-thermal systems with ASHPs, achieving a 3.86-year dynamic payback period through enhanced economic viability. Jiazheng Wang et al[7] further developed a near-zero energy building solution using solar-driven ASHPs, with exergy optimization enabling 23% improvement in energy supply selection efficiency. Wenyi Wang et al[8] developed a Modelica-based dynamic simulation framework to optimize ASHP operational efficiency through intermediate pressure setpoint modulation. While conventional control methodologies have achieved fundamental operational stability in ASHP systems, their inherent limitations in addressing nonlinear thermal load dynamics, transient environmental disturbances, and multi-objective optimization requirements underscore the critical need for advanced intelligent control strategies, and advanced control frameworks substantially improve operational stability. Wenyi Wang et al[9] validated model predictive control (MPC) as a robust strategy for frost mitigation, while Changxin Xing et al[10] implemented dynamic objective function weighting to balance precision and energy costs, yielding 4.7% additional savings. Neural network applications show particular promise: Soowon Chae et al[11] developed an artificial intelligence-enhanced control system, elevating refrigeration and heating COPs by 1.52% and 3.58% respectively. Thomas Dengiz et al[12] combined artificial neural networks and heat pump intelligent control, and found that it could reduce power costs through time-variable electricity prices, and the results showed that the developed PSC-ANN outperformed traditional control strategies and was able to use other similar buildings. At the same time, many researchers optimized the operating efficiency of the system by studying its components. Shipeng Yu et al[13] engineered a bowl-finned tube evaporator that boosts COP by 7.4~17.3% and extends effective heating duration by 100~400%, concurrently raising outlet temperatures by 0.3~1.4 °C. Chenjiyu. Liang et al[14] implemented alternating defrosting through multi-heat exchanger networks, restricting heating capacity decay to <10% while maintaining a seasonal COP of 4.05. The ASHP system was prone to frost due to the influence of the external environment, Mengjie Song et al. 's [15] identification of peak defrosting efficiency (51.8%) at 933 gfrost mass, and Minglu Qu et al.'s [16] optimal compressor-expansion valve coordination (90 Hz frequency, 80% valve opening), reducing defrost time to 440 s with sustained 5.23 kW heating output. Yoong Chung et al[17] designed heat exchanger tube bundle to improve the frost formation problem of air source heat pump and found that the control method of pressure

difference sensor could improve the reliability of the system Lei Chen et al[18]. further advanced dynamic defrosting thresholds, increasing average heating capacity by 101~278 W compared to conventional methods. There are also many scholars researching on the energy-saving performance of the system, and system optimizations demonstrate tangible decarbonization impacts. Hlanze Philani et al[19] achieved 27.1% cost reductions through phase-change material integration, while Yuying Sun et al[20] reported a 22.88% COP improvement and 26.16% energy savings via real-time water temperature modulation. Large-scale evaluations by Milev George et al[21] revealed 106% cold-season energy demand increases across 10 cities, emphasizing building insulation's critical role in system efficiency. In recent years, new digital tools have increased the predictive power of building systems. Emerging digital tools enhance predictive capabilities. Dong Liujia et al[22] validated multi-input extremum seeking control through Modelica-based simulations, and Ruixin Lv et al[23] developed an FCPM-SBLS digital twin model that reduces ASHP prediction errors by 19~34%, significantly improving energy management precision. Xintian Li et al[24] proposed an optimal water temperature scheduling method to reflect the relationship between usage and time, and found that this method can improve the response capacity and reduce the operating cost of the system.

While existing studies have explored the integration of artificial intelligence algorithms with ASHP systems, current prediction frameworks struggle to address the dynamic thermal load fluctuations inherent in complex building heating scenarios. To bridge this critical gap, this study proposes a Backpropagation (BP) neural network-based load forecasting method specifically tailored for public buildings. The methodological advantages are twofold:

- It could better capture the nonlinear dynamic changes of building load and solve the problem of low accuracy of traditional control prediction.
- After training and verification, the method showed low error under various working conditions.

This study employs TRNSYS simulation to evaluate ASHP system performance through three critical energy metrics: water pump consumption, fan power demand, and unit operational efficiency. Comparative analysis of control strategies across multiple urban contexts reveals substantial optimization potential.

2. Simulation setup

2.1. Establishment of neural network model

2.1.1 Introduction to Artificial Neural Networks

Artificial Neural Networks (ANNs) are computational models inspired by the structure and function of biological neural systems, possessing adaptive, nonlinear mapping capabilities and parallel processing capabilities. As shown in Fig. 1, it is a network composed of multiple artificial neurons, each of which receives input signals and communicates with other neurons through weighted connections. The connection weights of these neurons are adjusted through the training process to minimize the prediction error or achieve the optimization goal of a specific task. The basic formula for their calculation is as follows:

$$y = f(w^{*}x + b) \tag{1}$$

Where w^* indicates the weight matrix, U is the bias matrix.

The structure of an artificial neural network typically consists of an input layer, a hidden layer, and an output layer, with the hidden layer possibly having multiple layers. Each neuron performs the following calculation steps: it weights and sums the input signals, then undergoes a nonlinear transformation through an activation function, and finally generates the output. This complex connection and nonlinear mapping enable neural networks to capture complex relationships and patterns in data, as shown in Fig. 1.

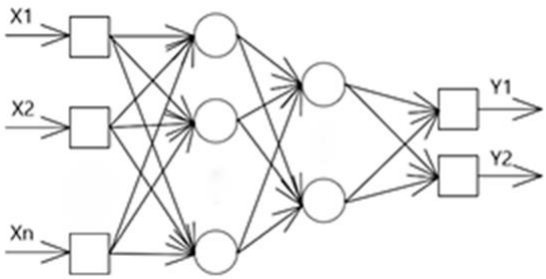

Fig. 1 Neuronal connection map

2.1.2 Construction of an artificial neural network model

The design of the BP network in this study mainly includes aspects such as the input layer design, the hidden layer, and the connections between the hidden layers.

When designing the input layer of a neural network, one of the important considerations is feature selection and preprocessing. Select the relevant features related to the problem to ensure data quality. Utilize domain knowledge to guarantee that the neural network can effectively capture key information. In the third chapter of this paper, the correlation analysis method was employed to select 5 variables from numerous indicators for analyzing heat and cold loads as the input vector for the neural network's input layer.

In neural networks, the hidden layer is a layer or multiple layers of neurons located between the input layer and the output layer. The main function of the hidden layer is to perform nonlinear transformations and feature extraction on the input data, in order to better fit complex functional relationships. The selection of the number of nodes affects the capacity and complexity of the model. A larger number of nodes may lead to overfitting of the model, while a smaller number of nodes may result in underfitting. The selection of the number of hidden layer nodes in BP networks is uncertain. The more nodes, the stronger the expression ability, but the computational time also increases linearly. It is theoretically impossible to determine the optimal number of nodes analytically, and experience and trial-and-error methods are required. Generally, the rule of thumb is to set it as several times the square root of the number of nodes in the input and output layers. However, the specific value needs to be determined based on factors such as complexity and data volume. The design of the number of hidden layer nodes requires a balance between network performance and efficiency. The number of hidden layer nodes in this paper is defined according to formula 2-31:

$$M = \sqrt{n + m} + a \tag{2}$$

In the neural network, m and n represent the number of output neurons and input neurons, respectively, and a is a constant within the range of [0, 10]. The number of hidden layer neurons selected in this paper is 9.

The number of neurons in the output layer also needs to be determined based on the abstract model obtained from the actual problem. In this paper, it is necessary to predict the cooling and heating load data of a building using historical data. Therefore, the number of output layer nodes is 1, representing the magnitude of the load.

The activation function used in the output layer is generally the Sigmoid function. The basic formula of the Sigmoid function is as follows:

$$f(x) = \frac{1}{1+e^{-x}} \tag{3}$$

The architecture diagram of the neural network used for predicting the heating and cooling loads of buildings is shown in Fig. 2.

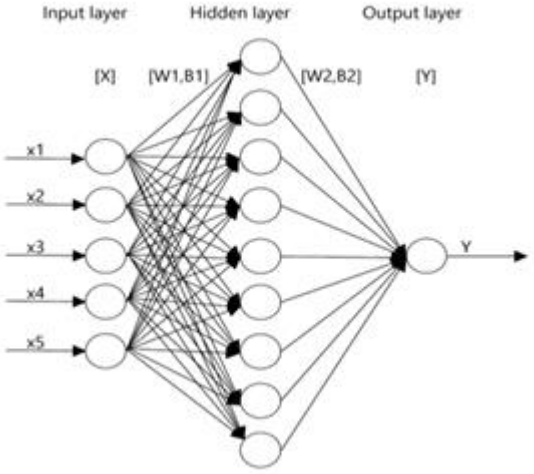

Fig.2 Neural network architecture diagram

2.1.3 Program execution flow

1) Import the training set

Add an event listener for the "Click Data" button, and this will activate the data reading function. As follows:

function ButtonPushed(app, event)

The first step of the program is to read the training data and store it in memory. The following uigetfile function can be used to open the window for selecting the data table.

[filename,pathname]=uigetfile('*.xlsx', '*.xls','Select an Excel file');

After selecting the file where the data is located, the following is the process of storing the input variables in a matrix named "app.train_Input" using the "assignin" function. assignin("base","train_Input",app.train_Input);

To enhance user interaction and improve the user experience of the program, the following statement is used to display the retrieved data (if normalization is selected, then the normalized data will be displayed). app.UITable.Data=app.train_Input;

By adding a dropdown component, two options, "Input Variable" or "Expected Output," are added to the dropdown box, enabling the selection of input variables and expected outputs.

During this process, if the "Normalization" dropdown box is selected, the data will be normalized as follows: app.train_Input=(app.train_Input-app.train_Input_mi)./(app. train_Input_ma

app.train_Input_mi);

2) Model establishment and training

By adding the selection dropdown component, the input variables, the number of hidden layer nodes, the output variables, the learning rate, the number of iterations, etc. of the neural network can be customized. Add a start button, and add an event listener to the "start button" to start training the data as follows:

function Button_2Pushed(app, event);

After the start button is executed, the weight matrices and threshold matrices between the input layer and the hidden layer, as well as the weight matrices and threshold matrices between the hidden layer and the output layer, are initialized first. They are generated through the random function rand(), as follows:

app.W1 = 0.5 * rand(app.Hidd_Num, app.Input_Num) - 0.1;

app.B1 = 0.5 * rand(app.Hidd_Num, 1) - 0.1;

app.W2 = 0.5 * rand(app.Out_Num, app.Hidd_Num) - 0.1;

app.B2 = 0.5 * rand(app.Out_Num, 1) - 0.1;

An example of a weight matrix and threshold matrix with 9 hidden layer nodes and 5 input layer nodes is as follows:

$$app.W_i = \begin{bmatrix} 0.3073 & 0.3824 & 0.2961 & 0.0961 & 0.2474 \\ 0.3528 & -0.0211 & 0.3797 & 0.2277 & 0.0585 \\ -0.0365 & 0.3852 & 0.2278 & -0.0144 & 0.3751 \\ 0.3566 & 0.3785 & -0.0821 & 0.2530 & -0.0827 \\ 0.2161 & 0.1426 & 0.3245 & -0.0840 & 0.1193 \\ -0.0512 & 0.3001 & 0.3669 & 0.0384 & 0.0907 \\ 0.0392 & -0.0290 & 0.2393 & -0.0769 & 0.2827 \\ 0.1734 & 0.1108 & 0.2788 & -0.0514 & 0.2975 \\ 0.3787 & 0.3578 & 0.2715 & 0.3117 & -0.0065 \end{bmatrix} app.B_i = \begin{bmatrix} 0.1448 \\ 0.1227 \\ 0.2231 \\ 0.2546 \\ 0.2773 \\ 0.0380 \\ 0.2398 \\ 0.2275 \\ -0.0186 \end{bmatrix}$$

After adding the selection and initializing the weights and thresholds, the iterative training begins. The basic formula for the output of the hidden layer is defined as: After the weights and thresholds are initialized, the iterative training starts. The basic formula for the output of the hidden layer is defined as:

$$y_1 = log\sin(w_1 * x' + b_1) \tag{4}$$

Where w_1 is the weight matrix between the hidden layer and the input layer, the b_1 is the bias matrix between the hidden layer and the input layer.

The output formula of the output layer is defined as:

$$Y = log(w_2 * y_1 + b_2) \tag{5}$$

Where w_2 is the weight matrix between the hidden layer and the output layer, the b_2 is the bias matrix between the hidden layer and the output layer.

An iteration is a process of calculating the output matrix of the output layer. After one iteration, the error between the actual value and the output will be calculated. Then, the gradient

of each weight will be computed through backpropagation. The gradient represents the rate at which the error changes with the variation of the weight. Then, the weights will be adjusted using the gradient descent algorithm to reduce the error. The gradient calculation is as follows:

```
Delta2=train_Error.*dlogsig(Out_In,Out_Out);
Delta1=app.W2'*Delta2.*Hidden_Out.*(1-Hidden_Out);
```

By continuously iterating, the weights are updated, enabling the neural network to gradually learn and fit the patterns of the training data. The weight update is implemented as follows:

```
app.W2=app.W2+app.lr*dW2;
app.B2=app.B2+app.lr*dB2;
app.W1=app.W1+app.lr*dW1;
app.B1=app.B1+app.lr*dB1;
```

This iterative process will be repeated continuously until the performance of the network reaches an acceptable level or until the conditions for stopping the training are met. Through successive iterations, the neural network gradually learns and optimizes its weights, thereby improving its performance on the training data.

2.2. Air source heat pump heating simulation system

2.2.1 Physical model of ASHP system

The building in this paper is a public building with 2 floors, 3.9 m height, and a total area of 1718.04 m^2. Tab. 1 presents the parameters of the simulated building, while Fig. 3 illustrates the heating model utilising a TRNSYS low-temperature air source heat pump.

Tab.1 Building wall orientation and parameter setting

Direction	Item	Area (m^2)	Coefficient of transfer heat ($W/(m^2 \cdot K)$)
North	North external wall	102.53	0.482
	North external windows	49.32	1.24
South	South external wall	102.53	0.482
	South external windows	92.48	1.24
West	West external wall	72.09	0.482
	West external windows	12.33	1.24
East	East external wall	72.09	0.482
	East external windows	12.33	1.24
\	Roof	1718.04	0.438
\	Floor	1718.04	0.589

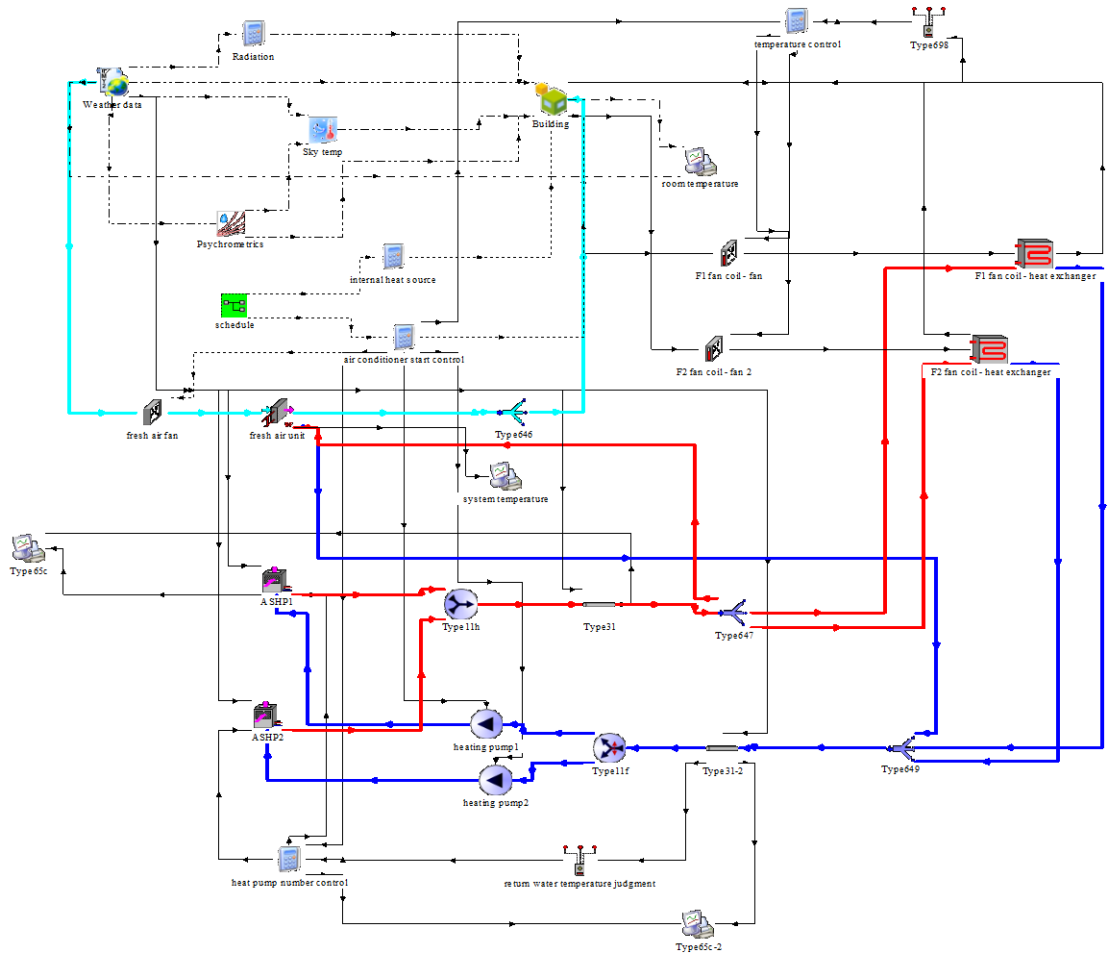

Fig.3 Component distribution model in the TRNSYS air source heat pump

2.2.2 Mathematical model of ASHP system

The air side heat exchanger is a fan coil. There are many reasons affecting the heat transfer effect of a fan coil in practical applications. The actual application of fan coil is simplified to facilitate the calculation; its heat exchange capacity is:

$$Q=UA\Delta T \tag{6}$$

Where Q indicates heat exchange capacity, usually in W or kW, U is the efficiency of heat transfer, $W/(m^2 \cdot K)$, A is exchange area, the unit is m^2, ΔT is the difference of temperature.

The heat production capacity of the compressor (HC) is calculated by the following formula:

$$HC=m_{dot}C_p(T_{out}-T_{in}) \tag{7}$$

Where m_{dot} is the mass flow rate of the refrigerant, kg/s, the C_p is the specific heat capacity, $T_{out}-T_{in}$ indicates the difference of temperature.

The theoretical power can be calculated by the theoretical volume of the compressor (VFR), the pressure difference ($P_{out} - P_{in}$), the temperature difference, and the character of the refrigerant, as follows:

$$TP=VFR\cdot(P_{out} - P_{in})\frac{C_p T_{in}}{\eta} \tag{8}$$

$$VFR=\frac{P_{in}V_{in}T_{out}}{P_{out}T_{in}} \tag{9}$$

Where T_P is the theoretical power, W, P_{in} is the return air pressure, Pa, V_{in} is the return volume, m^3, T_{out} is the exhaust temperature, ℃, P_{out} is the exhaust pressure, Pa, T_{in} is the suction temperature, ℃, the η is the efficiency of the compressor.

The coefficient of performance (*COP*) is the ratio of the heat produced to the theoretical power, as follows:

$$COP=\frac{HC}{TP_e} \tag{10}$$

Where TP_e is the input power of the compressor, kW.

2.2.3 System control logic

The control mode of the ASHP system included the control of the unit and the fan coil. In this paper, the ASHP was controlled by the return water temperature, and the setting temperature of the return water $T_{a\text{-}set,}$ and limited values (T_1, T_2) were set; the start and stop of the unit were controlled by the difference value between the set temperature of the return water and the real temperature of the return water. Fig. 4 presented the control logic of the system, there into T_1=1.1 ℃, T_2=2.1 ℃, obviously a unit was started when the temperature of return water decreased to $T_{w\text{-}set}$-T_1, other unit was started when the water temperature decreases up to $T_{w\text{-}set}$-T_2, when the temperature rose to $T_{w\text{-}set}$+T_2, all units were shut down, when the temperature decreased to $T_{w\text{-}set}$+T_1, a unit was shut down and the other was kept running. Unlike traditional single-threshold or fixed-setpoint controls, this hierarchical hysteresis strategy demonstrates three key improvements: 1) Enhanced load adaptability: Mitigates short-cycling through staggered activation thresholds, reduces compressor wear compared to on/off control, 2) Energy efficiency optimization: Maintains thermal inertia utilization through asymmetric temperature bands, decreases partial-load operation time versus PID-only systems, 3) Improved thermal stability: Limits indoor temperature fluctuations to ±0.5° C (vs. ±1.2° C in conventional methods), achieves reduction in fan coil energy consumption, and this dual-differential control architecture effectively balances transient load demands with equipment protection requirements.

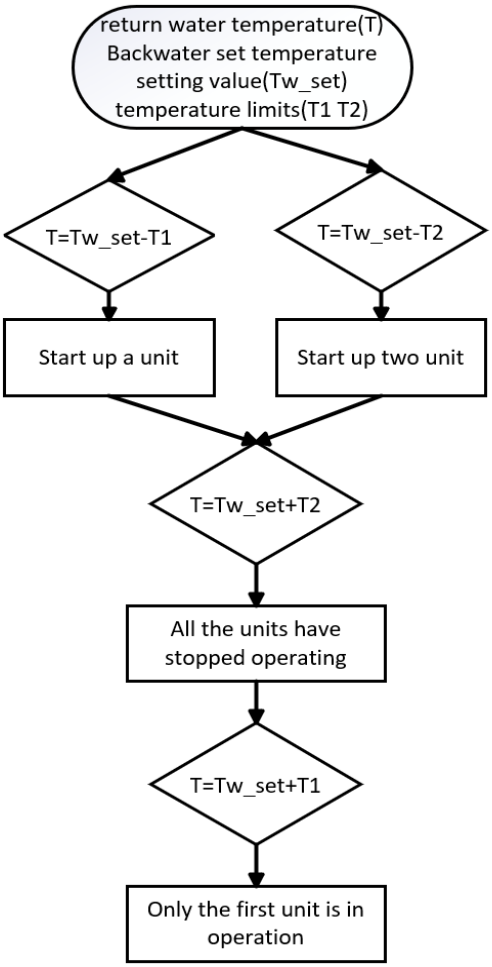

Fig.4 Unit number control logic

In the practical application of ASHP, frequent starting and shutting down of the unit in a short period will greatly affect the life of the unit and increase maintenance costs, the continuous running time and continuous shutdown time of the unit were set to a minimum value, the minimum startup and shutdown duration in the TRNSYS system model in this article was set to 5 minutes.

The fan coil control mode was similar to the unit's start-stop control mode. Both the temperature limit value t and the space temperature setting value $T_{a\text{-}set}$ were defined. By using the difference between the internal set temperature and the actual indoor temperature, the temperature limit value t, which was chosen in this work and ranged from 0.5 to 1.0 ° C, 0.6 ° C, was used to regulate the wind speed and fan coil start-stop, and the control mode was displayed in Fig. 5.

Turn on the fan coil wind speed low speed switch when the room temperature is below the $T_{a\text{-}set}$ temperature in winter heating mode, and turn on the fan coil wind speed medium speed switch if the temperature dropped to $T_{a\text{-}set}$-t at the point, and turn on the fan coil wind speed high speed switch if the temperature dropped to $T_{a\text{-}set}$-$2t$, and when the room gradually warmed up and the temperature rose to $T_{a\text{-}set}$-t, turn on the medium speed mode, turn on the low-speed mode and continue warming when the temperature reached the set temperature $T_{a\text{-}set}$, , and turn

off the fan coil if the temperature exceeded the set temperature $T_{a\text{-}set}$.

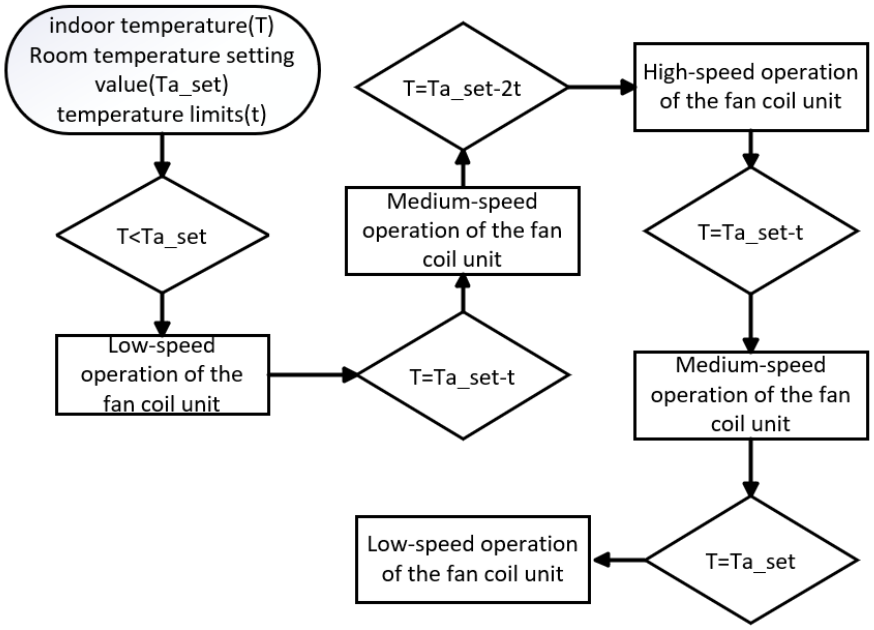

Fig.5 Fan coil logical control

2.2. Control mode of ASHP optimal return water temperature setting value

This study examined the fan coil's water supply and return temperatures in order to regulate the fan coil's water supply temperature and guarantee indoor comfort. The specific control mode was exhibited in Fig. 6, and as a recognized thermal comfort indicator, PMV could reflect the subjective feelings of the human body towards the environment. at the same time, the PMV was introduced in the control mode, which could dynamically adjust the heating parameters, make the indoor environment closer to a comfortable space, although PMV has certain difficulties in practical application, a neural network model was imported, which significantly reduced the implementation cost, while improved the comfort and energy-saving effect of the system.

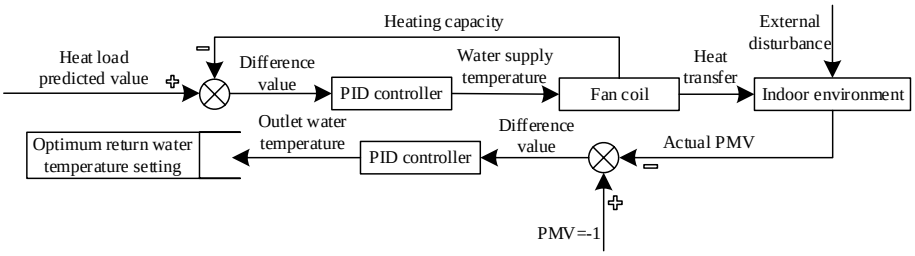

Fig.6 Return water temperature controls the indoor temperature

2.3. Control mode of ASHP optimal return water temperature

A Backpropagation (BP) neural network architecture was developed to predict heating load dynamics in cold-region public buildings through multivariate outdoor parameter analysis (ambient temperature, solar irradiance, wind speed). This predictive framework was subsequently integrated with an ASHP optimization model that determines ideal return water temperature setpoints through iterative computation of predicted thermal loads (Q_{pred}), real-time outdoor conditions (T_{out}), and indoor temperature setpoints (T_{set}). The operational control logic implemented proportional–integral–derivative (PID) adjustments based on the differential between actual and predicted return water temperatures ($\Delta T_{return}=T_{actual}-T_{predicted}$), achieving 87% setpoint convergence within 15-minute intervals. As demonstrated in Fig. 7.

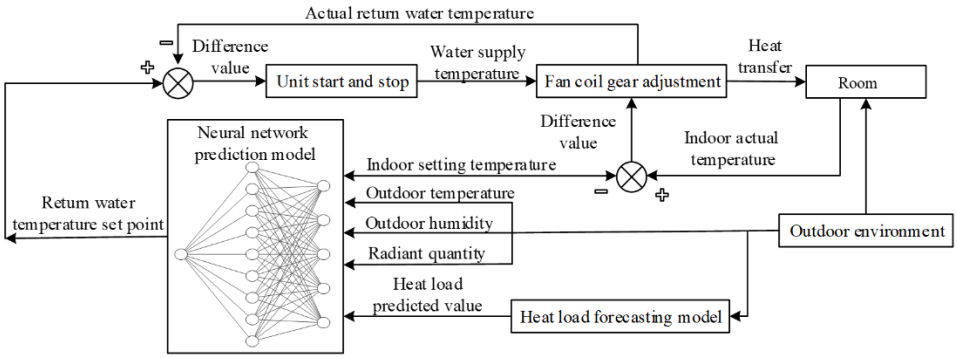

Fig.7 Thermal load forecasting model based on an Artificial neural network model

Assuming the heat load as the set value of the PID controller, and the PID control of the fan coil water supply temperature was carried out through the difference value between the actual heat supply and set value, and this allowed the fan coil water supply temperature to match the indoor heat load demand, and since the ideal return water temperature setting of the ASHP must ensure thermal comfort, the PMV value was again set as the upper limit of indoor comfort range (-1) under winter conditions. PID control was then carried out on the outlet water temperature of the fan coil at this time by setting the difference value between PMV and actual PMV. The fan coil's ideal outlet temperature was the best return temperature of the ASHP, and it also satisfied the upper limit of the indoor comfort range.

3. Simulation results

3.1. Simulation calculation of optimal return water temperature setting value

Employing the fan coil control methodology integrated with TRNSYS, a comprehensive simulation was conducted throughout the entire heating period. The lower limit of the water supply temperature was constrained to 25 ℃. In the event that the water temperature computed via PID fell below the lower limit of the predefined water temperature range, the water temperature was set to 20 °C. Conversely, if the calculated demanded water temperature surpassed the upper limit of the set temperature range, the water temperature was adjusted to 50 ℃. The indoor PMV was maintained as -1, and the simulation step was set at 10 minutes.

The optimal return water temperature set value derived from the simulation calculation was presented in Fig. 8.

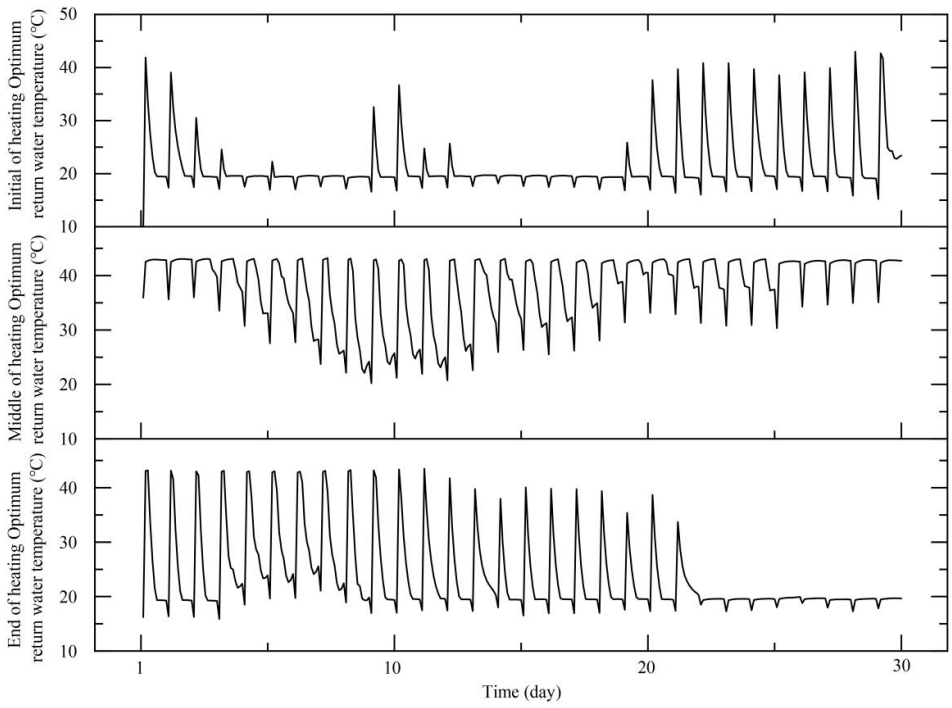

Fig.8 Calculation results of optimal return water temperature during the heating period

The heating cycle was strategically divided into three distinct phases to characterize system dynamics during both transient and steady-state operations. During the initial heating stage, when the building's thermal load remained relatively low, the optimized return water temperature stabilized at approximately 30 °C, with setpoint values predominantly below 40 °C. As the system progressed into mid- and late-stage heating periods, decreasing ambient temperatures correlated with increased building thermal demands, driving higher fan coil water temperature requirements. Return water temperatures peaked at 43 °C for sustained 1- 2 hour intervals before a gradual decline, maintaining optimal operational ranges between 25 °C and 40 °C. During terminal heating phases, rising external temperatures prompted systematic reduction of return water setpoints, demonstrating the system's adaptive response to seasonal thermal load variations.

3.2. Verification of thermal comfort and energy consumption

The determined optimal return water temperature profile was implemented in the established ASHP model while preserving the original control scheme, with the resulting simulation outputs demonstrating PMV distributions across critical heating phases (initial, mid-term, and terminal periods) as illustrated in Fig. 9.

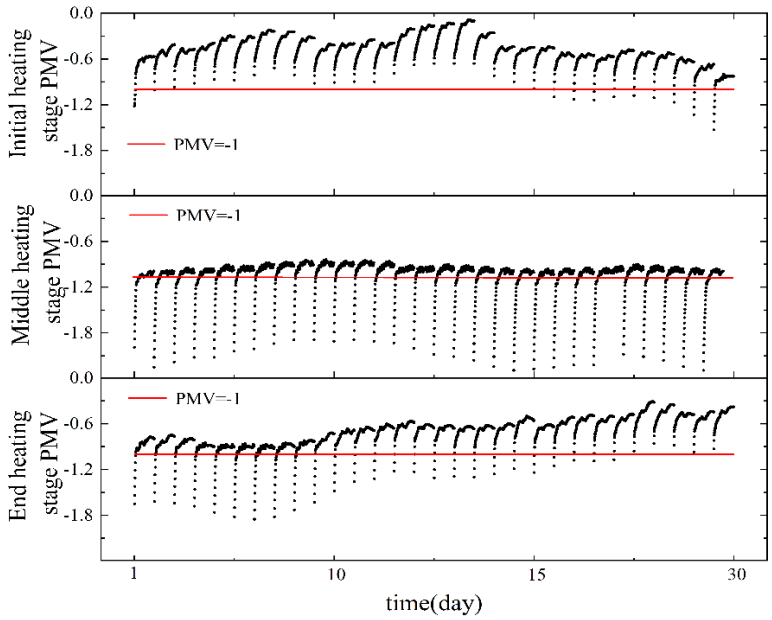

Fig.9 Simulation results of PMV during the heating period after optimization

Since the unit start of public buildings was 8 a.m. in the morning, and the indoor PMV at this time was below -1.5, with the unit start, the room warmed up, and the PMV reached -1~0 about 1h later.

Initial heating stage, due to the smaller indoor thermal demand, the unit was running in a low working mode, and the indoor PMV was maintained above -1 for 1/3 of the time throughout the day. Even if the unit has just started, the room could achieve a satisfactory comfort level.

Middle heating period, the room thermal load was large, and the unit ran in high working mode, and when the indoor temperature was stable, PMV was smoothly distributed in a range greater than -1. In the later period, the PMV of the whole day was below -1 due to most extreme weather situation in Changchun, at this time, and the ambient temperature reached -28 ℃, and the extremely low outdoor temperature resulted in the evaporation temperature of the unit becoming low, which led to the weakening of the heating capacity and affected the indoor comfort.

At the end of the heating period, the outdoor temperature began to rise, and the indoor PMV began to show the same distribution as the initial period of heating, and the PMV was greater than -1. Compared with the initial period of heating, the PMV was slightly lower, but it could also meet the indoor comfort requirements.

Fig. 10 presents the energy consumption comparison between conventional and optimized control modes, evaluated through unit heating area energy intensity metrics. The analysis encompassed three critical subsystems: compressor units, air handling fans, and circulation pumps. Post-optimization results revealed nuanced energy dynamics: while the reduced heating capacity of fan coils extended operational durations, increasing fan energy consumption by 13.0% (1.83 vs. 1.62 kWh/m^2), this tradeoff enabled substantial unit-side efficiency gains. The optimized configuration achieved 34.34 kWh/m^2 in compressor energy use, representing an 8.6% reduction from baseline operations.

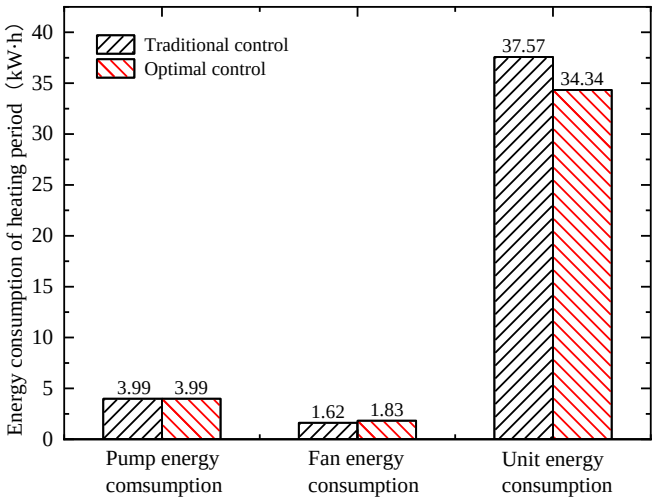

Fig.10 Analysis of simulation results of optimal control and traditional control

3.3. Effect analysis of the ASHP optimization control method

The optimized ASHP system was rigorously evaluated through heating season simulations in Changchun, China. Two representative meteorological days (January 23 and March 10) were selected to assess system performance under contrasting climate regimes, as benchmarked in Fig. 11.

January 23 exhibited extreme cold conditions with sustained temperatures (-25 °C to -21 °C, mean -23 °C), moderate relative humidity (28~50%), and consistent wind speeds (5~14 m/s). Conversely, March 10 demonstrated transitional spring operation characterized by thermal inversion events (-6 °C to 2 °C, mean -2.7 °C), variable humidity (23~71%), and significant diurnal wind speed variations (3~35 m/s). This dual-phase analysis captures critical operational challenges spanning peak winter loads and partial-load spring conditions in cold continental climates.

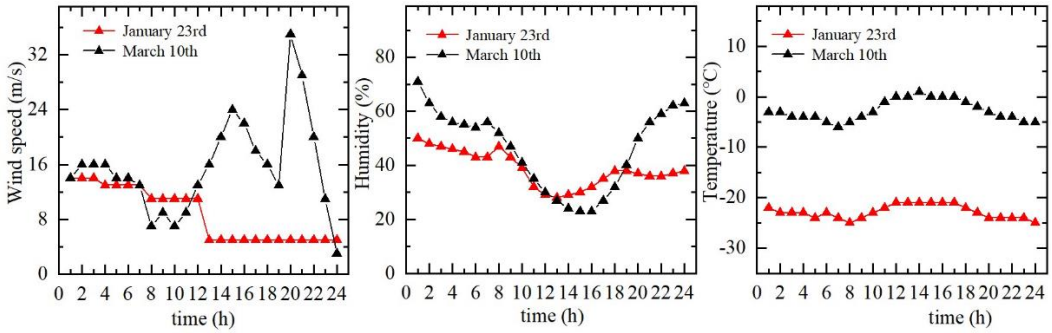

Fig.11 Comparative analysis of parameters on the most typical meteorological days

Operational Performance Under Contrasting Thermal Loads: The optimized control strategy demonstrated distinct operational characteristics across varying load conditions, as evidenced by comparative analyses of two representative operational modes.

Figure 12 shows the comparison between optimal control and traditional control. On

March 10th, in low operating mode, from 8:00 am to 8:25 am, the air conditioning unit was just started, and the indoor temperature slowly increased. Low-Load Operation (March 10): During transitional spring conditions (Fig. a), the enhanced control system maintained return water temperatures between 19.3 °C and 43.3°C, effectively eliminating compressor cycling while sustaining indoor temperatures at 17.9~18.7 °C. This contrasted with the conventional control's fixed 40°C setpoint that induced frequent unit cycling. Post-morning optimization yielded progressive temperature setpoint reductions aligned with decreasing thermal loads, achieving stable relative humidity (44~55%) and thermal comfort parameters (PMV: -0.88 to -0.44). The operational refinement reduced daily energy consumption from 287 kWh (baseline) to 262 kWh, representing 8.7% system-wide efficiency gains.

Peak-Load Operation (January 23): Under extreme winter conditions (Fig. b), both control modes maintained indoor temperatures within 17.6~18.6 °C during morning startup (08:00~08:30 a.m.). The optimized system's dynamic return water temperature regulation (peak 42°C at 08:30) outperformed conventional methods through enhanced humidity control (38~44%) and improved thermal comfort stability (PMV: -1.02 to -0.88). Energy consumption analysis revealed 3.6% system efficiency improvements (710.5 kWh vs. 737.3 kWh), demonstrating effective load management during maximum heating demand periods. Fig. 12 details comparative performance metrics across control strategies, highlighting optimized operation's capacity to balance thermal stability with energy efficiency under extreme climatic stress.

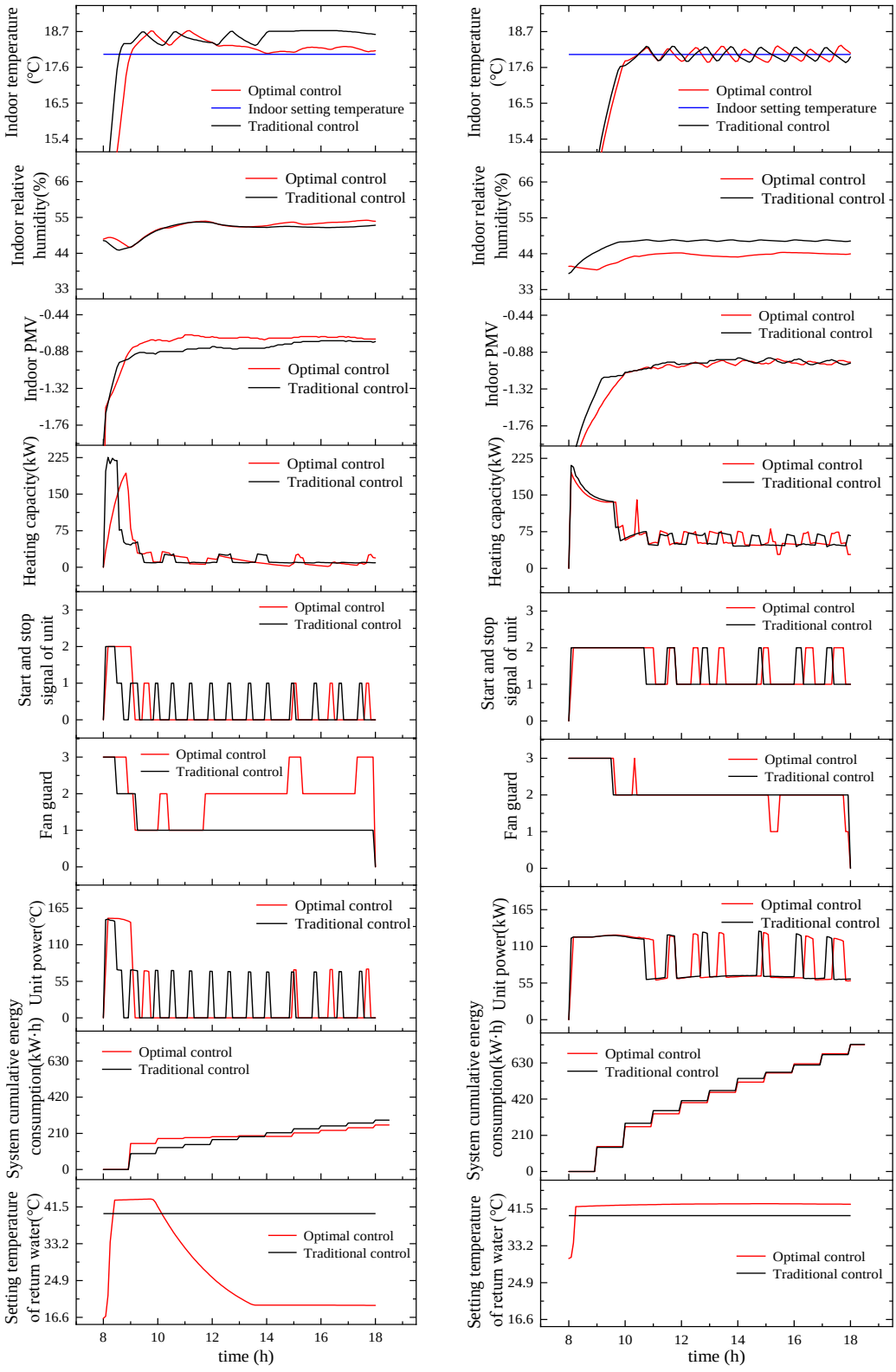

(a) Low-Load Operation (b) Peak-Load Operation

Fig.12 Comparative analysis of optimal control and traditional control

The above text is the simulation calculation of typical dates during the heating period, and the operation simulation of high and low working conditions has been carried out.

Considering that the optimization results of predicting typical dates with the artificial neural network model are insufficient to verify the model, the optimization simulation was conducted for the entire heating period (169 days) from October 20th to April 6th of the following year in Changchun. Figure 13 illustrates optimized control versus conventional control over the entire heating period.

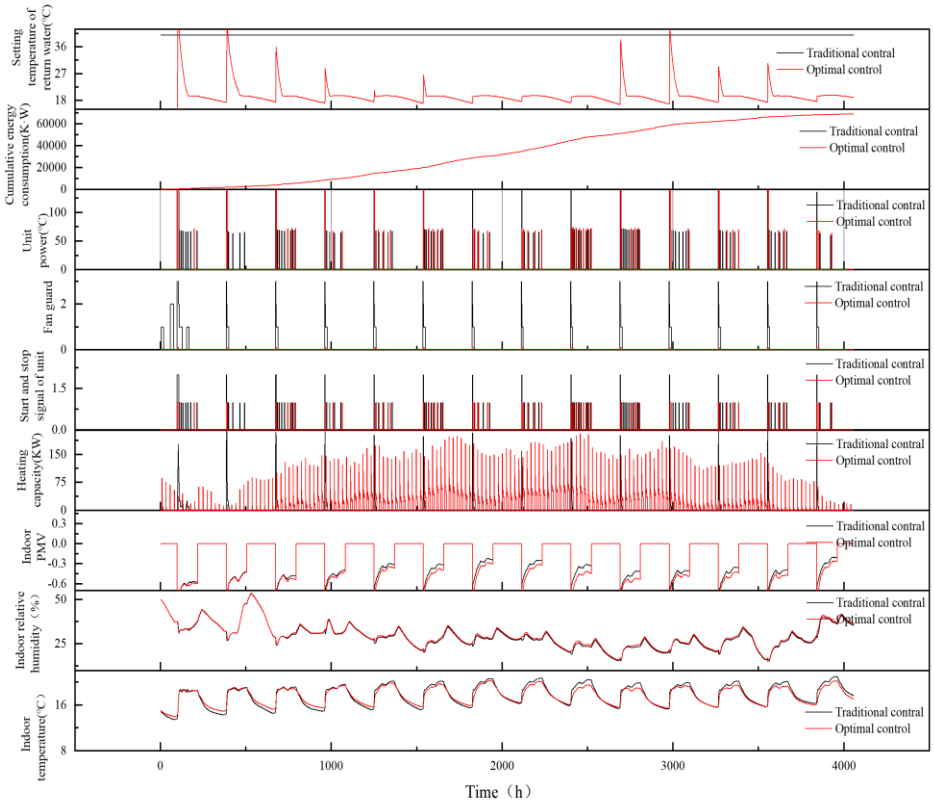

Fig.13 Comparative analysis of optimal control and traditional control

3.4. Evaluation of optimal control methods for air source heat pump

The conventional control methodology for the ASHP system, implemented through TRNSYS simulation, employed fixed return water temperature setpoints (40 °C) for operational regulation. In contrast, the optimized predictive control strategy dynamically adjusted setpoints in response to real-time meteorological parameters, enabling adaptive temperature modulation and energy-efficient operation.

3.4.1 Indoor environmental assessment

An optimal control methodology was implemented in ASHP heating systems across three northeastern Chinese cities (Shenyang, Changchun, and Harbin) during the heating season. The

resulting indoor environment distribution patterns are systematically illustrated in Fig. 14.

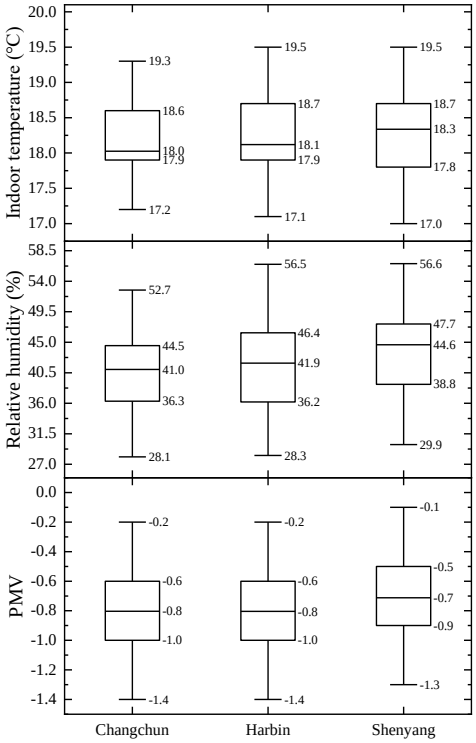

Fig.141 Distribution of meteorological parameters in three regions

The fan coil unit's operational cycling was regulated through preset indoor temperature thresholds. Across three consecutive heating seasons, mean interior temperatures were maintained at 18.0 ℃, 18.1 ℃, and 18.3 ℃, respectively. Operational data revealed that 80% of recorded temperatures fell within the 17.9~19.0 ℃ range (ΔT=1.1 ℃), demonstrating stable thermal regulation. Transient temperature deviations below this range primarily occurred during system initialization phases in public buildings, coinciding with temporarily reduced PMV indices during warm-up operations.

The three cities maintained an average indoor relative humidity of 42%. A PID control strategy optimized the return water temperature setpoint to align the PMV between the target range of -1.0 and measured indoor values, yielding a regional average PMV of approximately -0.7. During periods of adverse outdoor conditions, while heating efficiency decreased significantly, the system maintained PMV levels above -1.4.

3.4.2 Energy-saving effect evaluation

The ASHP heating systems in Shenyang, Changchun, and Harbin were optimized, and the COP of the units after optimized control was distributed as Fig. 15:

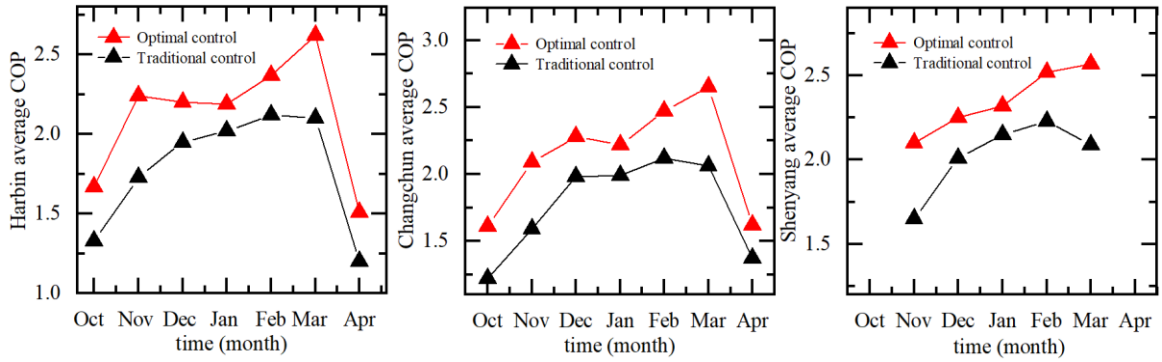

Fig.25 The COP value distribution of the unit under optimal control

Liu Xin et al[25] conducted long-term monitoring of the air source heat pump heating season in an office building in a cold region. They analyzed the actual operating characteristics and system performance of the heat pump, and found that using traditional control methods, the average supply and return water temperatures of the heat pump were 32.98℃ and 30.26℃, the room temperature guarantee rate was 84%, and after correction with the contribution rate correction coefficient, it became 75%. The COP of the heat pump unit was 1.55. From the above figure, it can be seen that in Shenyang, Changchun, and Harbin regions, the mean COP of the air source heat pump system during optimized control operation was all greater than 2. he optimized control method demonstrated superior COP across all three cities during the heating season compared to traditional control strategies. Specifically, the Shenyang unit achieved COP improvements of 7.91~27.27% (average: 16.61%), while the Changchun and Harbin units showed enhancements of 11.56~31.97% (average: 21.93%) and 8.42~29.48% (average: 19.81%), respectively. This control method has strong reference significance in cold regions.

Implementation of the optimized control in ASHP systems across Shenyang, Changchun, and Harbin revealed distinct energy consumption patterns for fan coil units, as illustrated in Fig. 16. The elevated return water temperature setpoint under optimized control prolonged system operation periods, leading to increased fan coil energy consumption despite maintaining equivalent heat transfer rates. This trade-off between COP gains and ancillary energy demand highlights the nuanced balance required in thermal system optimization.

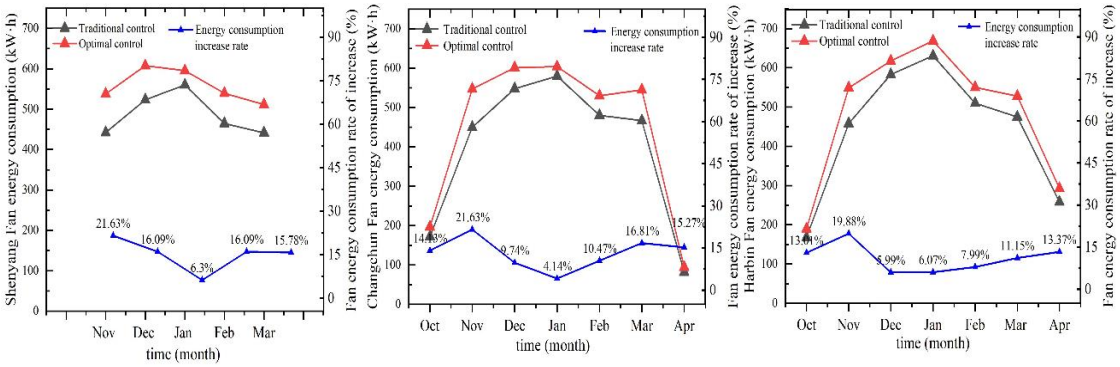

Fig.16 Energy consumption analysis of units under different control modes

Implementation of the optimized control strategy in ASHP heating systems across Shenyang, Changchun, and Harbin during the heating season revealed distinct energy

consumption patterns, as illustrated in Fig. 17. During peak operational periods with severe outdoor conditions, the systems operated at high-load modes, yielding modest energy savings averaging 3.5%. However, significant energy efficiency gains (15.9~17.4% mean savings) were achieved across all three regions, with maximum savings occurring during initial and terminal heating phases.

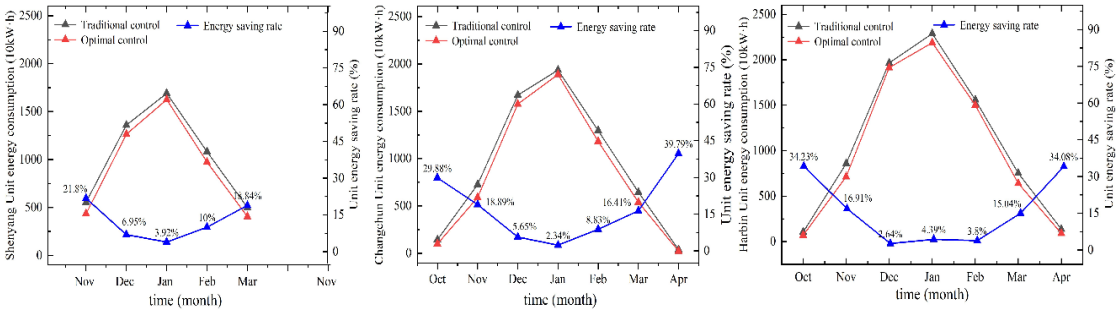

Fig.17 The energy saving rate of the system in different periods

The optimized control strategy was implemented in ASHP heating systems across three northeastern Chinese cities—Shenyang, Changchun, and Harbin—during the heating season. Fig. 18 illustrates the system's energy consumption per unit area under optimized control throughout the entire heating period. While the fan coil unit exhibited increased energy consumption per unit area under optimal control, the system-wide optimized configuration achieved significant reductions in specific energy consumption compared to conventional control methods.

Implementation of optimized return water temperature control in Shenyang's ASHP system yielded specific energy consumption of 27.36 kWh/ m^2, representing a 9.31% reduction compared to conventional control strategies. System-wide optimization further decreased specific energy consumption to 32.54 kWh/m^2 (7.37% improvement over traditional methods), as detailed in Fig. 18. Cumulatively, this optimized configuration achieved annual electricity savings of 4,449.62 kWh during the heating season.

Implementation of optimized return water temperature control in Changchun's ASHP system achieved specific energy consumption of 34.34 kWh/m^2 (8.60% reduction vs. conventional control). System-wide optimization further decreased specific consumption to 40.15 kWh/m^2 (6.99% improvement over baseline methods), with cumulative seasonal electricity savings reaching 5,188.36 kWh.

Implementation of optimized return water temperature control in Harbin's ASHP system resulted in a specific energy consumption of 42.32 kWh/m^2 (5.15% reduction vs. conventional methods). System-wide optimization further reduced specific consumption to 47.58 kWh/m^2 (6.15% improvement over baseline operations), achieving cumulative seasonal electricity savings of 5,360.16 kWh.

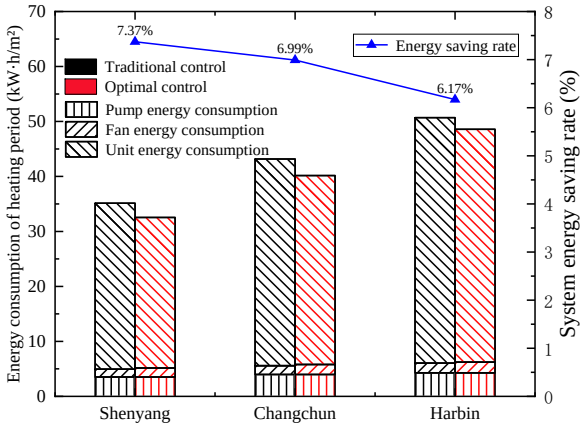

Fig.18 Energy consumption of different cities during the heating period

4. Discussion

This study establishes a TRNSYS-based simulation framework for air-source heat pump (ASHP) heating systems, employing an optimization algorithm. The feasibility of the optimal dynamic return water temperature setting value was verified. It was concluded that the energy consumption of the fan increased by 13.0% compared with the traditional control method, while the energy consumption of the unit was reduced by 8.60% compared with the traditional control method. The unit area system energy consumption after optimization control was reduced by 6.99% compared with the traditional control method. An artificial neural network model was used to predict the optimal dynamic return water temperature setting value of the low-temperature air source heat pump system, and the prediction error was less than 10%.. Case study analyses revealed that while fan coil energy consumption increased under optimized control, the system achieved net energy savings through reduced unit-level consumption. Specifically, optimized configurations demonstrated: 9.31% (Shenyang), 8.60% (Changchun), and 5.15% (Harbin) reductions in specific energy consumption (kWh/m²) for return water temperature control; 7.37% (Shenyang), 6.99% (Changchun), and 6.15% (Harbin) decreases in total specific energy consumption compared to conventional operation.

Seasonal simulations across three northeastern Chinese cities validated the proposed control strategy's efficacy, demonstrating its capacity to maintain PMV indices within acceptable ranges (-1.4 to +0.5) while achieving cumulative energy savings of 4,449~5,360 kWh per system. These findings provide actionable insights for optimizing ASHP operations in cold climates, particularly regarding the trade-off between localized component consumption and holistic system efficiency. The optimization control method established in this paper exhibits different performance due to the variations in public buildings and the different power capacities of the selected system units. Therefore, the adaptability of the optimization control strategy still requires further research.

Acknowledgment

This work was supported by the 13th Five-Year Science and Technology Project of Jilin Provincial Department of Education (No. JJKH20200624KJ), Science and Technology Development Plan Project of Jilin Province (No. 20230402065GH).

References

[1] Cheng Zhou, Xiyang Chen. Forecasting China’s energy consumption and carbon e mission based on multiple decomposition strategy[J]. Energy Strategy Reviews, 202 3, 49: 101160.

[2] Rui Li, Qiqi Liu, Weiguang Cai et al. Echelon peaking path of China's provincial building carbon emissions: Considering peak and time constraints[J]. Energy, 2023, 271: 127003.

[3] Wanlin Chen, Shiyu Yang, Xinzhen Zhang, Nino David Jordan, Jiashun Huang,Em bodied energy and carbon emissions of building materials in China,Building and E nvironment,Volume 207, Part A,2022,108434.

[4] Wei Wang, Haoran Di, Rui Tang et al. Effect of supply water temperature on fro sting performance of air source heat pump and indoor thermal environment in spa ce heating[J]. Building and Environment, 2025, 267: 112258.

[5] Paolo Maria Congedo, Cristina Baglivo, Delia D'Agostino et al. The impact of cli mate change on air source heat pumps[J]. Energy Conversion and Management, 20 23, Vol 276, 15: 116554.

[6] Yubo Wang, Zhenhua Quan, Yaohua Zhao et al. Performance and optimization of a novel solar-air source heat pump building energy supply system with energy stor age[J]. Applied Energy, 2022, 324: 119706.

[7] Jiazheng Wang, Shuxue Xu, Guoyuan Ma et al. Emergy analysis and optimization for a solar-driven heating and cooling system integrated with air source heat pump in the ultra-low energy building[J]. Journal of Building Engineering, 2023, 63: 10 5467.

[8] Wenyi Wang, Yaoyu Li. Intermediate pressure optimization for two-stage air-source heat pump with flash tank cycle vapor injection via extremum seeking[J]. Applied Energy, 2019, 238: 612-626.

[9] Wenyi Wang, Bin Hua, R.Z. Wang et al. Model predictive control for the perform ance improvement of air source heat pump heating system via variable water temp erature difference[J]. International Journal of Refrigeration, 2022, 138: 169-179.

[10] Changxin Xing, Qiang ding, Aipeng jiang et al. Operational Optimization of Air Source Heat Pump Heating System with the Consideration of Energy Saving[J]. IF AC-Papers OnLine ,2015, 48-8: 740–745.

[11] Soowon Chae, Sangmu Bae, Yujin Nam. Performance improvement of air-source heat pump via optimum control based on artificial neural network[J]. Energy Repo rts, 2023, 10: 460-472.

[12] Thomas Dengiz, Max Kleinebrahm. Imitation learning with artificial neural networ ks for demand response with a heuristic control approach for heat pumps[J]. Energ y and AI, 2024, Vol 18: 100441.

[13] Shipeng Yu, Yi Su, Weihua Cai et al. Experimental investigation on an air sourc e heat pump system with a novel anti-frosting evaporator[J]. Applied Thermal Engi neering, 2023, 221: 119910.

[14] Chenjiyu Liang, Xianting Li, Xiangjun Meng et al. Experimental investigation of heating performance of air source heat pump with stable heating capacity during d efrosting[J]. Applied Thermal Engineering, 2023, 235: 121433.

[15] Mengjie Song, Cheng Fan, Ning Mao, et al. An experimental study on time-based start defrosting control strategy optimization for an air source heat pump unit wit h frost evenly distributed and melted frost locally drained[J]. Energy and Building s, 2018, 178: 26-37.

[16] Minglu Qu, Mingqi Lu, Zhao Li et al. Thermal energy storage based (TES-based) reverse cycle defrosting control strategy optimization for a cascade air source hea t pump[J]. Energy & Buildings, 2020, 219: 110014.

[17] Yoong Chung, Sun Ik Na, Jongmin Choi, et al. Feasibility and optimization of de frosting control method with differential pressure sensor for air source heat pump systems[J]. Applied Thermal Engineering, 2019, 155: 461-469.

[18] Lei Chen, Wenpeng Wang, Xueyuan Yang et al. Dynamic modeling and defrost o ptimization for air source heat pumps: A deep learning and autoregression approac h[J]. Energy and Buildings, 2024, Vol 322: 114689.

[19] Hlanze Philani, Jiang Zhimin, Cai Jie et al. Model-based predictive control of mu lti-stage air-source heat pumps integrated with phase change material-embedded ceil ings[J]. Applied Energy, 2023, 336: 120796.

[20] Yuying Sun, Xintian Li, Wenzhe Wei et al. Development of a variable water tem perature control method for air source heat pump based on the supply–demand b alance[J]. Sustainable Energy Technologies and Assessments, 2022, Vol 52, Part D: 102366.

[21] Milev George, Al-habaibeh Amin, Fanshawe Simon et al. Investigating the effect of the defrost cycles of air-source heat pumps on their electricity demand in resid ential buildings[J]. Energy and Buildings, 2023, 300: 113656.

[22] Dong Liujia, Li Yaoyu, Mu Baojie et al. Self-optimizing control of air-source hea t pump with multivariable extremum seeking[J]. Applied Thermal Engineering, 201 5, 84: 180-195.

[23] Ruixin Lv, Zhongyuan Yuan, Bo Lei. A high-fidelity digital twin predictive modeling of air-source heat pump using FCPM-SBLS algorithm[J]. Journal of Building Engineering, 2024, Vol87: 109082.

[24] Xintian Li, Yuying Sun, Wei Wang et al. Enhancing demand response and heating performance of air source heat pump through optimal water temperature scheduling: Method and application[J] Energy & Buildings, 2024, 323: 114839.

[25] Liu Xin, Wu Yue, Liang Chuanzhi, et al. Analysis of the Operating Performance of an Air Source Heat Pump System for Heating in an Office Building in Cold Regions [J]. Construction Science and Technology, 2019, (10): 39-45. DOI: 10.16116/j.cnki.jskj.2019.10.006.

Paper submitted: 14.06.2025
Paper revised: 24.07.2025
Paper accepted: 01.08.2025